Journal of Science and Technology – Engineering and Technology for Sustainable Development
Volume 36, Issue 1, March 2026, 024–031

Room-Temperature Electrocaloric Enhancement in Barium Titanate Thin Films by Zirconium Doping

Ha Thi Dang [1,2]***, Ba-Hieu Vu*** [1]***, Dang Thi Hong Hue*** [1]***,***
Trong-Giang Nguyen [1]***, Van-Hai Dinh*** [1]***, Le Van Lich*** [1*]
[1] *School of Materials Science and Engineering, Hanoi University of Science and Technology, Ha Noi, Vietnam*
[2] *Vietnam National University of Forestry, Ha Noi, Viet Nam*
[*] *Corresponding author email: lich.levan@hust.edu.vn*

Abstract

The electrocaloric effect in ferroelectric materials has gained significant interest for the development of solid-state cooling devices. However, achieving a high electrocaloric effect near room temperature is still challenging. In the study, we employ a phase-field simulation approach to investigate the impact of zirconium (Zr) doping on the electrocaloric behavior of barium titanate zirconate, $BaZr_xTi_{1-x}O_3$ *(0% ≤ x ≤ 20%) ferroelectric thin films. Our results reveal that Zr doping significantly modifies the domain structures and phase transition dynamics, thereby enhancing the electrocaloric performance, particularly near room temperature. Isothermal entropy and adiabatic temperature variations are enhanced with increasing Zr doping content in* $BaZr_xTi_{1-x}O_3$ *thin films. The highest electrocaloric effect is observed in the* $BaZr_{0.2}Ti_{0.8}O_3$ *thin film, at near room temperature, corresponding to the transition from ferroelectric to paraelectric phase. Moreover, the* $BaZr_{0.2}Ti_{0.8}O_3$ *thin film also indicates a large entropy change at a low electric field and thus a large electrocaloric strength, which is beneficial for practical cooling at low voltages. These findings highlight the potential of Zr-doped* $BaTiO_3$ *thin films as promising candidates for energy-efficient solid-state cooling applications operating near room temperature.*

Keywords: Ferroelectric thin films, electrocaloric effect, phase transition, phase field model.

1. Introduction

The electrocaloric (EC) effect, which refers to a reversible adiabatic temperature change or isothermal entropy change in a dielectric material upon application of an electric field, has garnered significant interest as an energy-efficient mechanism for solid-state cooling [1]. Unlike conventional vapor-compression refrigeration, EC-based devices offer numerous advantages, including the absence of moving parts, environmental friendliness, high energy efficiency, and potential for miniaturization and integration into electronic devices [1]. Consequently, the development of ferroelectric materials exhibiting large EC responses near room temperature has become a crucial research focus for advancing EC-based refrigeration technologies. A central challenge in this field is the discovery of novel materials with enhanced EC properties, such as large entropy change (ΔS), significant adiabatic temperature change (ΔT), and low operating electric fields. Furthermore, a deep understanding and precise control of phase transitions, polarization dynamics, and microstructural features are essential for optimizing the EC performance of these materials.

The EC effect is fundamentally associated with the entropy change arising from the alignment of electric dipoles under an applied electric field, a phenomenon particularly pronounced in ferroelectric materials with spontaneous polarization [2]. Numerous studies have demonstrated that the magnitude, directionality, and reversibility of polarization under electric fields directly govern the entropy change and, consequently, the adiabatic temperature change observed during EC processes. Unlike bulk materials, thin films often exhibit altered polarization characteristics due to substrate-induced strain, interface effects, and size constraints. These factors can either enhance or suppress the EC response. For example, epitaxial strain in thin films has been successfully employed to stabilize ferroelectric phases with higher spontaneous polarization, leading to an amplified EC effect. Significant advancements have been reported in PZT and P(VDF–TrFE) thin films [3], which exhibited giant EC effects near room temperature under moderate electric fields. Therefore, understanding and controlling polarization behavior is paramount in tailoring the EC performance of ferroelectric thin films.

It is widely recognized that the EC effect in ferroelectrics reaches its peak near the Curie temperature (T_C), where the rate of change in polarization with temperature is at its maximum [4].

---

p-ISSN 3093-3242
e-ISSN 3093-3579
https://doi.org/10.51316/jst.188.etsd.2026.36.1.4
Received: May 28, 2025; Revised: Jul 4, 2025
Accepted: Jul 11, 2025; Online: Feb 5, 2026.

A major challenge, however, is that the T_C of many common ferroelectric materials is significantly above room temperature, limiting their direct use in practical cooling applications. As a result, substantial effort has been directed toward developing methods to tailor the EC properties to enhance the temperature change around room temperature, including techniques such as particle size reduction, strain engineering, rare-earth doping, and compositional modification near morphotropic phase boundaries [5, 6].

Doping is a highly effective method for tailoring the ferroelectric and EC properties of materials. In particular, doping barium titanate ($BaTiO_3$) with zirconium (Zr) has shown considerable promise for reducing the phase transition temperature and modifying polarization behavior [7]. The incorporation of Zr into the $BaTiO_3$ lattice alters the energy landscape of the ferroelectric domains, weakens long-range dipole-dipole interactions, and can induce diffuse phase transitions. These effects broaden the temperature range of the EC response and enhance the EC coefficient, especially at lower temperatures. Indeed, experimental studies have confirmed that Zr doping in $BaTiO_3$ not only shifts the Curie temperature toward room temperature but also increases the dielectric tunability and polarizability under an external electric field [7, 8].

In addition, recent advancements have highlighted the role of domain engineering in enhancing the electrocaloric (EC) response of ferroelectric materials. By tailoring domain configurations such as increasing domain wall density, promoting closure domains, and manipulating nanoscale domain structures significant improvements in polarization magnitude and reversibility under electric fields have been achieved. These microstructural optimizations are particularly vital in ferroelectric thin films, where interface effects, doping concentration, and size constraints strongly influence domain stability and switching dynamics. Consequently, understanding the interplay among doping concentration, domain morphology, and phase transition behavior is essential for designing high-performance EC materials. Phase-field modeling offers a powerful approach to simulate the thermodynamic and kinetic processes governing domain evolution and EC effects. By incorporating composition-dependent parameters, the model can accurately predict how Zr doping alters the ferroelectric properties of $BaTiO_3$ thin films, offering a pathway for systematic optimization of EC performance near room temperature.

In this study, we systematically investigate the influence of Zr doping on the EC properties of $BaTiO_3$ thin films using a phase-field simulation approach. We demonstrate that increasing the Zr concentration significantly modifies the ferroelectric domain structure and phase transition behavior, leading to enhanced isothermal entropy change (ΔS) and adiabatic temperature change (ΔT). Notably, we find that the EC effect is maximized near room temperature in films with 20% Zr doping, where a broadened phase transition and stabilized polar domains contribute to a strong EC response. Our findings provide valuable insights for optimizing lead-free ferroelectric materials for advanced solid-state cooling technologies.

2. Methods

2.1. The Component Equations of Energy

A phase-field model is constructed for $BaZr_xTi_{1-x}O_3$ (BZTx) thin films to simulate the evolution of polarization domain structures and examine the hysteresis loops for various film compositions. The phase field model is described in the Cartesian coordinate system $x_1x_2x_3$, where vector components are denoted by subscript indices (1, 2, 3). For example, p_1, p_2, and p_3 represent the components of the polarization vector along the x_1, x_2, and x_3 axes, respectively. In the phas-field model, three primary variables are used to describe the domain structures and their responses to external fields, namely the spontaneous polarization p_i (i=1,2,3), the displacement u_i, and the electric potential φ. Their gradients determine the polarization gradient $p_{i,j}$, the strain tensor ε_{ij}, and the electric field E_i, as [9]:

$$p_{i,j} = \frac{\partial p_i}{\partial x_j} \tag{1}$$

$$\varepsilon_{ij} = \frac{1}{2}\left(\frac{\partial u_i}{\partial x_j} + \frac{\partial u_j}{\partial x_i}\right) \tag{2}$$

$$E_i = \frac{\partial \varphi}{\partial x_i} \tag{3}$$

The electric enthalpy for BZTx is given by [9].

$$f = f_{\mathrm{Landau}}(p_i) + f_{\mathrm{Grad}}(p_{i,j}) + f_{\mathrm{Elas}}(p_i, \varepsilon_{ij}) + f_{\mathrm{Elec}}(p_i, E_i)$$

where $f_{\mathrm{Landau}}(p_i)$, $f_{\mathrm{Grad}}(p_{i,j})$, $f_{\mathrm{Elas}}(p_i, \varepsilon_{ij})$, and $f_{\mathrm{Elec}}(p_i, E_i)$ are Landau, gradient, elastic, and electrostatic energy densities, respectively. The Landau energy density of BZTx is described by an eighth-order polynomial [9]:

$$\begin{gathered} f_{\mathrm{Landau}}(p_i) = \alpha_1(p_1^2 + p_2^2 + p_3^2) \\ +\alpha_{11}(p_1^4 + p_2^4 + p_3^4) \\ + \alpha_{12}(p_1^2p_2^2 + p_2^2p_3^2 + p_3^2p_1^2)\ \alpha_{111}(p_1^6 + p_2^6 + p_3^6) \\ +\alpha_{112}[p_1^4(p_2^2 + p_3^2) + p_2^4(p_1^2 + p_3^2) + p_3^4(p_1^2 + p_2^2) \\ +\alpha_{123}p_1^2p_1^2p_1^2 + \alpha_{1111}(p_1^8 + p_2^8 + p_3^8 + \alpha_{123}p_1^2p_1^2p_1^2 \\ +\alpha_{1112}[(p_1^6(p_2^2 + p_3^2) + p_2^6(p_1^2 + p_3^2) \\ +p_3^6(p_1^2 + p_2^2)] \\ +\alpha_{1123}(p_1^4p_2^2p_3^2 + p_1^2p_2^4p_3^2 + p_1^2p_2^2p_3^4) \end{gathered} \tag{5}$$

where α_i, α_{ij}, α_{ijk}, and α_{ijkl} represent thermodynamic (or Landau) coefficients. The total free energy comprises the contribution of domain walls, which arises from the gradient of the polarization field. This polarization gradient energy density is given by [9]:

$$f_{\mathrm{Grad}}(p_{i,j}) = \frac{1}{2}G_{11}\left(p_{1,1}^2 + p_{2,2}^2 + p_{3,3}^2\right) + G_{12}\left(p_{1,1}^2 p_{2,2}^2 + p_{2,2}^2 p_{3,3}^2 + p_{1,1}^2 p_{3,3}^2\right) + \frac{1}{2}G_{44}\left[\begin{matrix}\left(p_{1,2} + p_{2,1}\right)^2 + \left(p_{2,3} + p_{3,2}\right)^2 \\ + \left(p_{1,3} + p_{3,1}\right)^2\end{matrix}\right] + \frac{1}{2}G'_{44}\left[\begin{matrix}\left(p_{1,2} - p_{2,1}\right)^2 + \left(p_{2,3} - p_{3,2}\right)^2 + \\ \left(p_{1,3} - p_{3,1}\right)^2\end{matrix}\right] \quad (6)$$

where G_{ij} are gradient coefficients. The elastic energy density is expressed as [9]:

$$f_{\mathrm{Elas}}(p_i, E_i) = \frac{1}{2}c_{ijkl}(\alpha_{ij} - \alpha_{ij}^0)(\alpha_{kl} - \alpha_{kl}^0) \quad (7)$$

where c_{ijkl} are elastic coefficients that are evaluated at fixed eigenstrain. The α_{ij}^0 eigenstrain caused by the polarization field is expressed as [9]

$$\begin{aligned}\alpha_{11}^0 &= Q_{11}p_1^2 + Q_{12}(p_1^2 + p_3^2), \quad \alpha_{23}^0 = Q_{44}p_2p_3 \\ \alpha_{22}^0 &= Q_{11}p_2^2 + Q_{12}(p_1^2 + p_3^2), \quad \alpha_{13}^0 = Q_{44}p_1p_3 \\ \alpha_{33}^0 &= Q_{11}p_3^2 + Q_{12}(p_1^2 + p_2^2), \quad \alpha_{12}^0 = Q_{44}p_1p_2\end{aligned} \quad (8)$$

where Q_{ij} are the electrostrictive coefficients. The electrostatic energy density is described by [9]:

$$f_{\mathrm{Elec}}(p_i, E_i) = -\frac{1}{2}\,\kappa_c(E_1^2 + E_2^2 + E_3^2) - (E_1p_1 + E_2p_2 + E_3p_3) \quad (9)$$

where κ_c is the dielectric parameter.

The mechanical equilibrium condition is given by [9]:

$$\nabla.\sigma = \frac{\partial}{\partial x_i}\left(\frac{\partial f}{\partial \varepsilon_{ij}}\right) = 0 \quad (10)$$

The electric equilibrium is given by [9]:

$$\epsilon_0 \epsilon_{ij}^b \nabla_i \nabla_j \varphi = p_{i,i}, \quad (11)$$

where ϵ_0 is the vacuum permittivity, and ϵ_{ij}^b is the relative background permittivity. The temporal evolution of the polarization field is determined by solving the time-dependent Ginzburg–Landau (TDGL) equation, as [9]:

$$\frac{\partial p_i(x_i,t)}{\partial t} = -M\frac{\partial F}{\partial p_i(x_i,t)}, \quad (12)$$

where M is the mobility coefficient, t is the evolution time, and $F = \int_V f dV$ is the total energy of the ferroelectric system with volume V.

2.2. Modeling and Simulation Methods

This work focuses on B-site substituted BZT*x*, a solid solution system composed of the tetragonal ferroelectric BTO and the paraelectric $BaZrO_3$ (BZO). At room temperature, the BZT*x* solid solution exhibits a composition-dependent single-phase transition from the ferroelectric tetragonal phase to the paraelectric cubic phase, with the Zr content (x) serving as a key control parameter. Within this system, the lattice parameters and the Curie temperature (T_C) display an approximately linear variation between the values of pure BTO and BZO end-members. Notably, the Curie temperature of BZT*x* can be effectively tuned across a broad temperature range by adjusting the Zr content. As the Zr content is increased, the polarization weakens, and T_C is gradually decreased due to the reduction of long-range dipolar interactions and the enhancement of fluctuations originating from the BZO composition. In addition, BZT*x* solid solutions exhibit relatively high pyroelectric coefficients near the morphotropic phase boundary, while maintaining low dielectric losses, making them attractive candidates for EC cooling applications. Taking advantage of the inverse electrothermal conversion inherent to the pyroelectric effect, large EC effects can be realized in BZT*x* near room temperature.

To explore these phenomena, we simulate the EC response of BZT*x* with varying material compositions using a three-dimensional phase-field model. The simulation domain is a volume of 128 × 2 × 64nm³, with periodic boundary conditions applied along the x_1 and x_2 directions to mimic an extended thin film. The system is spatially discretized using a regular grid with a uniform grid spacing of $\Delta x_1 = \Delta x_2 = \Delta x_3 = 1.0$ nm. The coordinate axes, x_1, x_2, and x_3, are aligned with the [100], [010], and [001] crystallographic directions, respectively. The compositionally dependent material parameters for BZT*x* are taken from previous studies [9] and listed in Table 1. The equilibrium domain structures in BZT*x* are then obtained by iteratively solving the TDGL equation. The simulations are initiated from a random polarization configuration and evolve until the total free energy converges to a stable minimum. Equations (10) to (12) that govern the phase-field model are numerically solved using a spectral method based on fast Fourier transforms [9]. Note that the phase field model used in this study is established by using our in-house subroutine, which is developed from (10) to (12).

Once the polarization configuration achieves thermodynamic equilibrium, we apply a quasi-static electric field along the x_3 direction to probe the polarization switching behavior as a function of temperature. Specifically, the temperature is systematically varied from 0 °C to 150 °C in increments of 10 °C to capture the full temperature dependence of the polarization response.

Table 1. Material coefficients of BZTx with various Zr concentrations [9], given in SI units and temperature T in K)

Coefficients	Magnitudes
α_1 (10^5 C^{-2} m^{2}N)	$5.0\times(160[\mathrm{Coth}(160/T)-\mathrm{Coth}(160/390)]+\lambda_1 x)$
α_{11} (10^8 C^{-4} m^{6}N)	$-1.1542\ (1+\lambda_2 x)$
α_{12} (10^8 C^{-4} m^{6}N)	$6.5300\ (1+\lambda_2 x)$
α_{111} (10^9 C^{-6} m^{10}N)	$-2.1063\ (1+\lambda_3 x)$
α_{112} (10^9 C^{-6} m^{10}N)	$-4.0909\ (1+\lambda_3 x)$
α_{123} (10^9 C^{-6} m^{10}N)	$-6.6879\ (1+\lambda_3 x)$
α_{1111} (10^{10} C^{-6} m^{10}N)	$7.5896\ (1+\lambda_4 x)$
α_{1112} (10^{10} C^{-6} m^{10}N)	$-2.1927\ (1+\lambda_4 x)$
α_{1122} (10^{10} C^{-6} m^{10}N)	$-2.2206\ (1+\lambda_4 x)$
α_{1123} (10^{10} C^{-6} m^{10}N)	$2.4159\ (1+\lambda_4 x)$
λ_1	$-3.51-\tanh[10^3(x-0.175)](1694.50x^2-696.18x+6.03)$
	$-3.51+\tanh[10^3(x-0.175)](-1714.28x^2+264.59x-56.88)$
λ_2	$\begin{cases}-1.12-19.6x & \text{if } 0<x\le 0.175\\ 29.75-196x & \text{if } 0.175<x\le 0.3\end{cases}$
λ_3	0
λ_4	$-9\lambda_2$
c_{11} (10^{-12} m^{2}N^{-1})	$8-3-4.87x$
c_{12} (10^{-12} m^{2}N^{-1})	$-2.7+2.025x$
c_{44} (10^{-12} m^{2}N^{-1})	$9.24+5.05x$
Q_{11} (C^{-2} m^4)	$0.1-0.004x$
Q_{12} (C^{-2} m^4)	-0.034 - $0.005x$
Q_{44} (C^{-2} m^4)	$0.029+0.002x$

The reversible change of internal energy in the BZTx thin film is governed by the fundamental laws of thermodynamics and can be related to the electrocaloric effect through the appropriate Maxwell relations [10]. Thus, the isothermal entropy change (ΔS) and the adiabatic temperature change (ΔT) can be computed via the following expressions [10].

$$\Delta S=-\int_{E_a}^{E_b}\frac{1}{\rho}\left(\frac{\partial P}{\partial T}\right)_E dE, \tag{13}$$

$$\Delta T=-\int_{E_a}^{E_b}\frac{T}{\rho c_p}\left(\frac{\partial P}{\partial T}\right)_E dE, \tag{14}$$

where ρ is the density of material, c_p denotes the specific heat capacity at constant pressure, and E_a and E_b correspond to the initial and final value of the applied electric fields, respectively. In the present study, we set the initial field to zero (E_a = 0). Given the calculated variation of the polarization with temperature, the values of ΔS and ΔT are then estimated by performing numerical integration of (13) and (14).

3. Results and Discussion

3.1. Domain Structures in BaZr$_x$Ti$_{1-x}$O$_3$ Thin Films

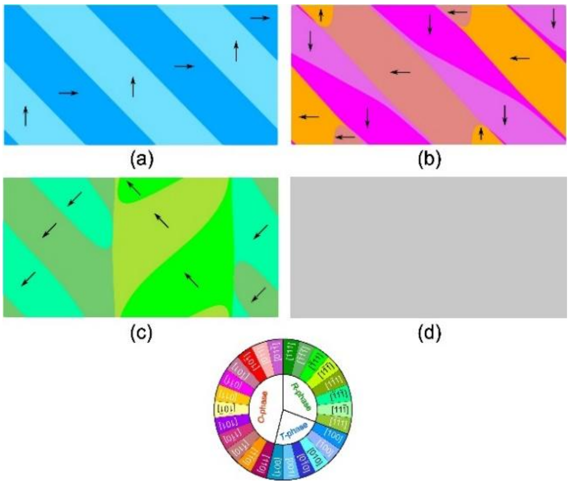

Fig. 1. Spontaneous polarization domain structures of BaZr$_x$Ti$_{1-x}$O$_3$ thin films at different Zr concentrations: (a) x = 0%, (b) x = 5%, (c) x = 10%, and (d) x = 20%

Fig. 1 depicts the domain structures of BZT*x* thin films at room temperature, for a range of Zr contents (*x* = 0%, 5%, 10%, and 20%). As the Zr content is increased, significant evolution in the polarization domain patterns is observed, reflecting the influence of Zr on the underlying phase stability and polarization behaviors. Specifically, the BZT*x* thin films exhibit a progression of ferroelectric phases for *x* less than 20%, transitioning from the tetragonal to orthorhombic, and then to rhombohedral symmetry. At higher doping levels, for *x* greater than 20%, the films adopt a cubic or paraelectric phase, indicating the suppression of long-range ferroelectric order. At *x* equal 0%, the film forms regular, parallel 90° stripe domains, a characteristic feature of the tetragonal ferroelectric phase, as shown in Fig. 1a. The polarization vectors within these domains are predominantly aligned along the <100> directions, adopting a head-to-tail configuration to minimize electrostatic energy. The characteristics of the 90◦ stripe domain configuration are in good agreement with previous experimental reports and simulation studies for BTO thin films [11]. Increasing the Zr content to *x* equal 5% (Fig. 1b) leads to a change in preferred polarization orientation, with the polarization now aligning along the <110> crystallographic axes. This indicates a phase transition to the orthorhombic phase. The domain configurations become more complex and disordered, with the initial straight stripe domains exhibiting increased curvatures and distortion. Furthermore, the domain walls become less sharp, and regions with continuously varying polarization begin to emerge. At a higher Zr content of *x* equal 10% (Fig. 1c), the domain structure further evolves into a highly curved and irregular stripe configuration and dispersion. This reflects the dominance of the rhombohedral phase with a high degree of polarization anisotropy, which is consistent with the presence of relaxor-like behavior in the material. Remarkably, when the Zr content is further increased to *x* equal 20% (Fig. 1d), the ferroelectric domain completely disappears, and the net polarization vanishes throughout the film. This signifies a complete transition to the cubic paraelectric phase, where long-range ferroelectric order is no longer stable. Note that a previous study [9] on the phase transition of BZT*x* reported that the material undergoes a first-order phase transition, characterized by an abrupt change from the ferroelectric to the paraelectric phase. As a result, the coexistence of ferroelectric and paraelectric phases is unlikely to be observed at room temperature in our simulation. These observations demonstrate that precise control over the Zr doping concentration in BZT*x* thin films provides a means to selectively stabilize distinct crystallographic phases, namely the tetragonal, orthorhombic, rhombohedral, and cubic phases. These structural transformations, driven by composition, have a profound impact on the electrocaloric and dielectric properties of the BZT*x* system.

3.2. Polarization Behavior under External Fields

To comprehensively assess the influence of Zr doping on the EC behavior of BZT*x* thin films, we examined the temperature-dependent polarization in thin films with varying Zr concentrations (*x* = 0%, 5%, 10%, and 20%). Fig. 2 illustrates that the polarization-temperature (P_3-T) relationships obtained under different electric fields (E_3) for the first quadrant of the P_3-E_3 hysteresis loops at various temperatures for the BZT*x* thin films. All films exhibit a decreasing trend in polarization with increasing temperature under applied electric fields ranging from 0 to 100 kVcm^{-1}, consistent with the expected thermal depolarization behavior of ferroelectric materials. In the undoped BTO thin film (*x*=0%), the polarization exhibits a sharp decrease with increasing temperature in the absence of an electric field, reaching near-zero values above 120 °C. This indicates a sharp ferroelectric-to-paraelectric phase transition, a characteristic behavior of classical ferroelectrics. The near-zero polarization observed in the undoped BTO thin film near 120 °C confirms the appearance of the paraelectric phase, consistent with previous reports [9]. Under an applied electric field of E_3 = 30 kVcm^{-1}, a significant decrease in polarization with increasing temperature is still observed, although the polarization does not reach zero. This behavior suggests the persistence of field-induced polarization even above the Curie temperature, a common phenomenon in ferroelectric systems where external fields stabilize the ferroelectric state. When a higher electric field is applied to the undoped BTO thin film, the polarization becomes less sensitive to temperature, and at any given temperature, the average polarization increases with increasing electric field.

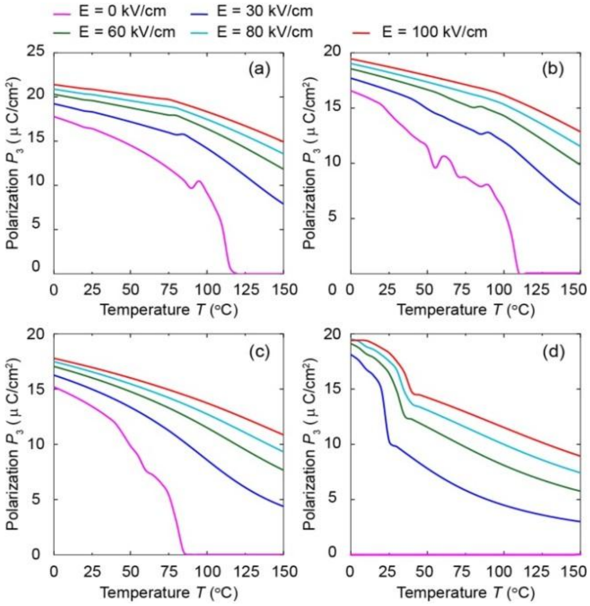

Fig. 2. Temperature dependence of the polarization of BZT*x* thin films with various Zr contents under different electric fields: (a) *x* = 0%, (b) *x* = 5%, (c) *x* = 10%, and (d) *x* = 20%

Similar trends in the temperature dependence of polarization are observed in Fig. 2(b) to Fig. 2(d) for the BZT*x* thin films with higher Zr contents. Notably, as the Zr content increases, the Curie temperature (T_C), defined as the temperature at which the polarization magnitude approaches zero in the absence of an electric field, shifts towards lower temperatures. Specifically, as the Zr content increases from 5% to 20%, the polarization-temperature (P_3-T) curves gradually broaden, and the sharp phase transition becomes more diffuse. This broadening of the transition and the shift of T_C toward lower values, approaching room temperature, are characteristic features of ferroelectric relaxor behavior. Such materials, due to local compositional disorder and the presence of polar nano-regions, exhibit a distribution of transition temperatures rather than a single, well-defined T_C. This behavior is reflected in the increasingly smooth P_3-T curves observed at higher doping levels. Therefore, increasing the Zr content in BZT*x* thin films effectively reduces the Curie temperature of the material, bringing it closer to room temperature. This result aligns with experimental observations for BZT*x* thin films [12]. Furthermore, the reduced sensitivity of polarization to temperature under higher electric fields in doped BZT*x* films suggests improved thermal stability of the ferroelectric state. This is advantageous for practical EC cooling applications, as the ability to induce and sustain polarization over a broad temperature range enhances the potential cooling power and operating temperature range of the EC effect.

3.3. Effect of Zr Contents on the Electrocaloric Properties

To investigate the EC effect and evaluate the influence of Zr doping on the thermo-electrical response of BZT*x* thin films, we analyze the EC effect in BZT*x* films with varying material compositions. The isothermal entropy change (ΔS) and adiabatic temperature change (ΔT) as functions of temperature are calculated for the BZT*x* thin films under various electric field changes, based on the polarization-temperature curves and employing Maxwell's relations (13) and (14). The electric field change was defined as $\Delta E = E_b - E_a$ ($E_a = 0$). Fig. 3 and Fig. 4 present the temperature dependences of ΔS and ΔT for different applied electric fields (30, 60, 80, and 100 kVcm^{-1}) for the BZT*x* thin films doped with 0%, 5%, 10%, and 20% Zr. The EC effect exhibits a strong dependence on both the Zr content and the applied electric field.

In Fig. 3a, the undoped BTO thin film displays a sharp peak in ΔS as a function of temperature, centered around 120 °C, corresponding to its Curie temperature ($T_C \approx 393$ K). When the electric field change by 30 kVcm^{-1}, the maximum entropy change reaches a value of 2.85 Jkg^{-1}K^{-1}. In the BZT5 film, multiple peaks in ΔS are observed (Fig. 3b). At $\Delta E_3 = 30$ kVcm^{-1}, ΔS reaches a first peak value of 1.38 Jkg^{-1}K^{-1} at 55 °C. Subsequent peak values are 1.05 Jkg^{-1}K^{-1} at 70 °C, 1.18 Jkg^{-1}K^{-1} at 85 °C, and 2.44 Jkg^{-1}K^{-1} at 115 °C, respectively. Notably, a negative entropy change ($\Delta S < 0$) appears near 75 °C at higher electric fields, reflecting the instability of the polar domains as the material undergoes intermediate phase transitions. It is important to note that the ΔS peak observed near 115 °C, close to the phase transition temperature, is present in both undoped BTO and BZT5 films. At this temperature, the magnitude of the ΔS peak is higher in the undoped BTO film than in the BZT5 film. In the BZT10 film (Fig. 3c), ΔS gradually increases with increasing temperature for $T < 85$ °C (except for the temperature range from 70 to 85 °C), but decreases when $T > 85$ °C. Under $\Delta E_3 = 30$ kVcm^{-1}, ΔS reaches a maximum value of 2.15 Jkg^{-1}K^{-1} at 85 °C. Compared to both the undoped BTO film and the BZT5 film, the BZT10 film exhibits smaller ΔS values at lower temperatures. Remarkably, for the BZT20 film (Fig. 3d), the isothermal entropy change reaches a maximum value of 5.3 Jkg^{-1}K^{-1} at 20 °C under an electric field change of 30 kVcm^{-1} and 7.5 Jkg^{-1}K^{-1} under an electric field change of 100 kVcm^{-1}, indicating a significant shift of the EC peak toward lower temperatures. This result is expected, as the entropy change is typically highest near the phase transition temperature, and the Curie temperature decreases as the Zr content increases. The high entropy change at near-room temperature is a desirable feature for solid-state cooling applications and confirms that Zr doping effectively enhances the EC response at lower temperatures.

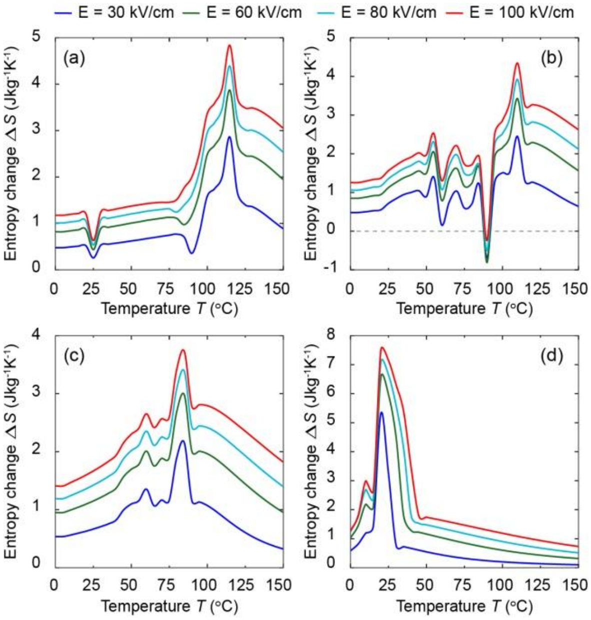

Fig. 3. Temperature dependence of the isothermal entropy change of the BZT*x* thin films with different material compositions: (a) $x = 0\%$, (b) $x = 5\%$, (c) $x = 10\%$, and (d) $x = 20\%$.

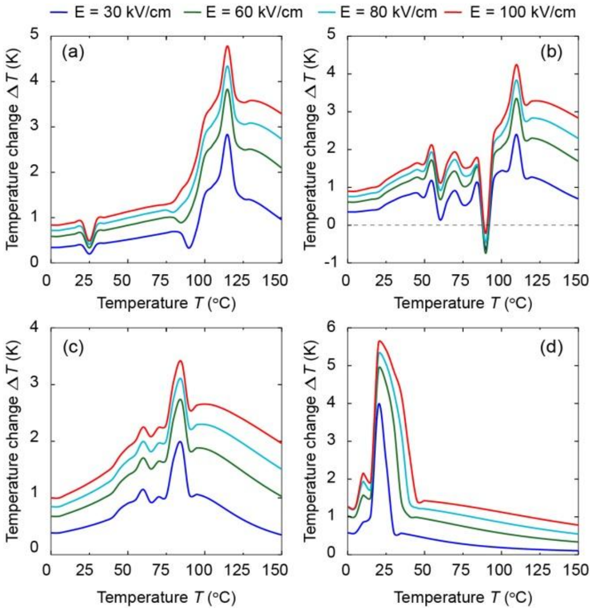

Fig. 4. Temperature dependence of the adiabatic temperature change of the BZT*x* thin films with different material compositions: (a) $x = 0\%$, (b) $x = 5\%$, (c) $x = 10\%$, and (d) $x = 20\%$.

For all films, increasing the applied electric field change (ΔE) leads to an increase in ΔS. Notably, the peak values of ΔS occur at the same temperature, regardless of the applied electric field. A larger ΔE also improves the stability of ΔS over a range of temperatures. In Fig. 4(a), for the undoped BTO film under ΔE = 30 kVcm^{-1}, the adiabatic temperature change (ΔT) peaks at 2.82 K at 115 °C, then gradually decreases with increasing temperature. At a larger electric field change of ΔE = 60 kVcm^{-1}, ΔT peaks at 3.82 K at 115 °C. Comparing ΔT under different electric field changes, a larger ΔE enhances the stability of ΔT over temperature, which is crucial for utilizing the EC effect in varying operating temperature ranges. The temperature at which ΔT reaches its maximum value remains constant, irrespective of the applied electric field. Similar trends in ΔS and ΔT are observed in the other BZT*x* thin films, as shown in Figs. 4(b) to Fig. 4(d). Remarkably, the highest peak value of ΔT, occurring at the lowest temperature (near room temperature), is observed in the films with higher Zr content ($x = 20\%$). Furthermore, increasing the applied electric field change (ΔE) leads to a higher ΔT. Specifically, under ΔE = 30 kVcm^{-1}, the ΔT of BZT5 and BZT20 achieves magnitudes of 2.39 K and 3.96 K, respectively. Under ΔE = 60 kVcm^{-1}, ΔT of BZT5 and BZT20 achieves magnitudes of 3.34 K and 4.89 K, respectively. Therefore, increasing the Zr doping concentration in the BZT*x* thin films not only reduces the Curie temperature but also increases the adiabatic temperature change, making these materials more suitable for room-temperature electrocaloric cooling applications.

Although the temperature dependence of ΔS and ΔT exhibits similar trends, they represent distinct thermodynamic processes. ΔS quantifies the change in entropy when an electric field is applied under isothermal conditions, providing insight into the amount of heat absorbed or released by the system. In contrast, ΔT denotes the change in temperature during an adiabatic application or removal of the electric field, directly reflecting the cooling performance of electrocaloric materials in solid-state cooling devices.

4. Conclusion

In summary, this study demonstrates that zirconium doping significantly enhances the electrocaloric effect in barium titanate ferroelectric thin films. The substitution of Zr^{4+} ions into the Ti^{4+} sites effectively modifies the domain structure, broadens the ferroelectric-paraelectric phase transition, and enhances polarization dynamics under applied electric fields. Consequently, Zr-doped $BaTiO_3$ films exhibit a larger adiabatic temperature change and entropy variation compared to undoped $BaTiO_3$, particularly near room temperature, making them promising candidates for practical solid-state cooling applications. Furthermore, zirconium doping improves the isothermal entropy change at low electric fields, enhancing the suitability of these films for integration into microscale cooling devices. Our findings highlight the potential of compositional engineering, specifically Zr doping, as an effective strategy to optimize the electrocaloric performance of ferroelectric thin films. This work provides a valuable foundation for further development of high-efficiency, lead-free electrocaloric materials and devices, paving the way for advanced solid-state cooling technologies.

Acknowledgments

This research is funded by Vietnam National Foundation for Science and Technology Development (NAFOSTED), under Grant No. 103.02-2021.79.

References

[1] X. Moya, S. Kar-Narayan, and N.D. Mathur, Caloric materials near ferroic phase transitions, Nature Materials, vol. 13, no. 5, pp. 439–450, Apr. 2014. https://doi.org/10.1038/nmat3951

[2] F. Weyland, A. Bradeško, Y. B. Ma, J. Koruza, B. X. Xu, K. Albe, T. Rojac, and N. Novak, Impact of polarization dynamics and charged defects on the electrocaloric response of ferroelectric Pb(Zr,Ti)O_3 ceramics, Energy Technology, vol. 6, iss. 8, pp. 1519–1525, May 2018. https://doi.org/10.1002/ente.201800140

[3] T. Zhang, W. Li, W. Cao, Y. Hou, Y. Yu, and W. Fei, Giant electrocaloric effect in PZT bilayer thin films by utilizing the electric field engineering, Applied Physics Letters, vol. 108, no. 16, p. 162902, Apr. 2016. https://doi.org/10.1063/1.4947446

[4] X. Wei, C. Zhao, T. Zheng, X. Lv, L. Zhang, B. Li, and J. Wu, Understanding the enhanced electrocaloric effect in $BaTiO_3$-based ferroelectrics at critical state, Acta Materialia, vol. 227, p. 117735, Apr. 2022. https://doi.org/10.1016/j.actamat.2022.117735

[5] J. Qiu and Q. Jiang, Grain size effect on the electrocaloric effect of dense $BaTiO_3$ nanoceramics, Journal of Applied Physics, vol. 105, no. 3, p. 034110, Feb. 2009. https://doi.org/10.1063/1.3063811

[6] Z. Wang, M. Yang and H. Zhang, H., Materials, Strain engineering on electrocaloric effect in $PbTiO_3$ and $BaTiO_3$, Advanced Composites and Hybrid Materials, vol. 4, no. 4, pp. 1239–1247, Apr. 2021. https://doi.org/10.1007/s42114-021-00257-6

[7] M. Reda, S. El-Dek, and M. Arman, Improvement of ferroelectric properties via Zr doping in barium titanate nanoparticles, Journal of Materials Science: Materials in Electronics, vol. 33, pp. 16753–16776, Jun. 2022. https://doi.org/10.1007/s10854-022-08541-x

[8] S. J. Kuang, X. G. Tang, L. Y. Li, Y. P. Jiang, and Q. X. Liu, Influence of Zr dopant on the dielectric properties and Curie temperatures of $Ba(Zr_xTi_{1-x})O_3$ ($0\leq x\leq 0.12$) ceramics, Scripta Materialia, vol. 61, iss. 1, pp. 68–71, Jul. 2009. https://doi.org/10.1016/j.scriptamat.2009.03.016

[9] Y. H. Huang, J.-J. Wang, T. N. Yang, X. X. Cheng, B. Liu, Y. J. Wu, L.-Q. Chen, Thermodynamic and phase-field studies of phase transitions, domain structures, and switching for $Ba(Zr_xTi_{1-x})O_3$ solid solutions, Acta Materialia, vol. 186, no., pp. 609–615, Mar. 2020. https://doi.org/10.1016/j.actamat.2020.01.019

[10] P. Thacher, Electrocaloric effects in some ferroelectric and antiferroelectric $Pb(Zr,Ti)O_3$ compounds, Journal of Applied Physics, vol. 39, no. 4, pp. 1996–2002, Mar. 1968. https://doi.org/10.1063/1.1656478

[11] A. S. Everhardt, S. Matzen, N. Domingo, G. Catalan, B. Noheda, Ferroelectric domain structures in low-strain $BaTiO_3$, Adv. Electron. Mater, vol. 2, iss. 1, p. 1500214, Nov. 2015. https://doi.org/10.1002/aelm.201500214

[12] A. Dixit, S. Majumder, A. Savvinov, R. Katiyar, R. Guo, A. Bhalla, Investigations on the sol–gel-derived barium zirconium titanate thin films, Materials Letters, vol. 56, iss. 6, pp. 933–940, Nov. 2002. https://doi.org/10.1016/S0167-577X(02)00640-7